The Astrophysical Journal, 631:988–1000, 2005 October 1

CONSTRAINTS ON GRAIN FORMATION AROUND CARBON STARS FROM LABORATORY STUDIES OF PRESOLAR GRAPHITE

Thomas J. Bernatowicz, Onaolapo Wali Akande, Thomas K. Croat, and Ramanath Cowsik
Department of Physics, Washington University, Campus Box 1105, One Brookings Drive, St. Louis, MO 63130-4899;
tom@wustl.edu, owal@wustl.edu, tkc@wuphys.wustl.edu, cowsik@wuphys.wustl.edu
Received 2005 March 8; accepted 2005 June 2

ABSTRACT

We report the results of an investigation into the physical conditions in the mass outflows of asymptotic giant branch (AGB) carbon stars that are required for the formation of micron-sized presolar graphite grains, with and without previously formed internal crystals of titanium carbide (TiC). A lower mass limit of 1.1 $M_{\odot}$ for stars capable of contributing grains to the solar nebula is derived. This mass limit, in conjunction with a mass-luminosity relation for carbon stars, identifies the region of the H-R diagram relevant to the production of presolar graphite. Detailed dynamical models of AGB outflows, along with constraints provided by kinetics and equilibrium thermodynamics, indicate that grain formation occurs at radii from 2.3 to 3.7 AU for AGB carbon stars in the 1.1–5 $M_{\odot}$ range. This analysis also yields time intervals available for graphite growth that are on the order of a few years. By considering the luminosity variations of carbon stars, we show that grains formed during minima in the luminosity are likely to be evaporated subsequently, while those formed at luminosity maxima will survive. We calculate strict upper limits on grain sizes for graphite and TiC in spherically symmetric AGB outflows. Graphite grains can reach diameters in the observed micron size range (1–2 μm) only under ideal growth conditions (perfect sticking efficiency, no evaporation, no depletion of gas species contributing to grain growth), and then only in outflows from carbon stars with masses $\lesssim$2.5 $M_{\odot}$. The same is true for TiC grains that are found within presolar graphite, which have mean diameters of 24 $\pm$ 14 nm. In general, the mass-loss rates that would be required to produce the observed grain sizes in spherically symmetric outflows are at least an order of magnitude larger than the maximum observed AGB carbon star mass-loss rates. These results, as well as pressure constraints derived from equilibrium thermodynamics, force us to conclude that presolar graphite and TiC must form in regions of enhanced density (clumps, jets) in AGB outflows having small angular scales. As shown in the companion paper by Croat et al., the enrichment of ^{12}C in many AGB graphites, and the overabundances of the *s*-process elements Mo, Zr, and Ru in the carbides found within them, often greatly exceed the values observed astronomically in AGB outflows. These observations not only lend further support to the idea that the outflows are clumpy, but also imply that the outflowing matter is not well mixed in the circumstellar envelope out to the radii where grain condensation takes place.

Subject headings: dust, extinction — stars: AGB and post-AGB — stars: carbon

1. INTRODUCTION

Insight into the nature of circumstellar dust has traditionally come from astronomical observations, but in recent years the laboratory study of presolar grains has emerged as a rich complementary source of information not only about its nature but about the conditions of its formation. Presolar grains are found in primitive meteorites and interplanetary dust particles, and are minerals that condensed prior to the formation of the solar system in the mass outflows from red giant stars, novae, and supernovae (SNe). They are identified as presolar on the basis of isotopic ratios in both major and minor elements that differ substantially from the solar ratios in a way that cannot have resulted from nuclear reactions, radioactive decays, or isotopic fractionation within the solar system. Many species of presolar minerals have been identified, and these include silicates (Messenger et al. 2003; Nguyen & Zinner 2004); various magnesium, titanium, and aluminum oxides; nanodiamonds; graphite; silicon carbide; silicon nitride; solid solutions of refractory Ti, V, Fe, Zr, Mo, and Ru carbides; and Fe-Ni and Fe-Ru metals present as subgrains within presolar graphite (see Daulton et al. 2003 and references therein).

Presolar grains are studied by a variety of microanalytical techniques in the laboratory, so their compositions and physical properties can be well characterized and may be used to obtain specific astrophysical information. Studies of the isotopic composition of individual grains by the ion microprobe, interpreted with the aid of nucleosynthesis models and astrophysical data, help to identify the specific types of stellar sources in whose mass outflows the grains condensed, and yield insights into stellar nucleosynthesis at an unprecedented level of detail (see Bernatowicz & Walker 1997; Bernatowicz & Zinner 1997; Zinner 1998; Nittler 2003; Clayton & Nittler 2004). The results of mineralogical, microchemical, and microstructural studies of presolar grains with transmission electron microscopy (TEM) not only give unambiguous information about the kinds of astrophysical solids that actually form, but with the help of kinetic and thermochemical models may also be used to infer the conditions of grain condensation in circumstellar dust shells (Lodders & Fegley 1995, 1997a; Sharp & Wasserburg 1995; Bernatowicz et al. 1996; Bernatowicz & Cowsik 1997; Daulton et al. 2002, 2003) and SN outflows (Croat et al. 2003). In addition, because the grains must have traversed the interstellar medium (ISM) prior to their incorporation into the solar nebula, they serve as monitors of physical and chemical processing of grains in the ISM (Bernatowicz et al. 2003).

In the present work we analyze the laboratory data on presolar graphite grains to derive astrophysical information about the conditions of grain formation around asymptotic giant branch (AGB) stars. This work is motivated by several factors.

First is the availability of a greatly expanded data set based on correlated isotopic, chemical, and structural microanalyses of individual presolar graphite grains that have been performed since our previous treatment of this subject nearly a decade ago (Bernatowicz et al. 1996). These observations are presented in the companion paper by Croat et al. (2005; hereafter Paper I). Second, advances in nucleosynthesis models and in the isotopic analysis of individual presolar grains by secondary ion mass spectrometry have led to improved constraints on possible stellar sources of presolar graphite (see § 2). Third, greatly improved astronomical constraints on the masses, radii, pulsation periods, and luminosities of Galactic carbon stars have since been provided in part by analyses of data from the *Hipparcos* (Perryman 1997) mission. Fourth, there have been substantial improvements in the self-consistent treatment of radiative transfer and hydrodynamics in circumstellar envelopes. In the present work we use these improved observations and models, as well as constraints provided by equilibrium thermodynamics and kinetics, in a semiempirical evaluation of the physical conditions that are required for the growth of the presolar graphite grains in the atmospheres of carbon AGB stars.

2. STELLAR SOURCES OF PRESOLAR GRAPHITE

Bernatowicz et al. (1996) previously conducted ion microprobe and TEM studies of presolar graphite spherules from the Murchison meteorite KFC1 graphite separate (number weighted mean diameter $\sim$1–2 μm; 2.15–2.20 g cm^{-3}; Amari et al. 1994) that revealed the presence of internal refractory carbides (Ti, Zr, Mo, and Ru carbides and their solid solutions) in some graphites. The TEM observations were used in conjunction with detailed equilibrium condensation calculations for a gas of solar composition (except for enhanced C/O and *s*-process elements; Lodders & Fegley 1995; Sharp & Wasserburg 1995) to infer pressures, C/O gas ratios, and temperatures during grain formation. Chigai et al. (2002) also used these observations in a study of the kinetics of heterogenous nucleation in stellar atmospheres.

Bernatowicz et al. (1996) concluded from thermodynamic considerations that the condensation of refractory carbides prior to graphite required an *s*-process enrichment of Zr and Mo of at least 30 times their solar proportions. One plausible stellar source of the carbide-containing graphites is therefore low-mass ($\sim$1–3 $M_\odot$) asymptotic giant branch (AGB) carbon stars, particularly N type, that typically have *s*-process enrichments of heavy elements (e.g., Zr, Ba, and rare earth elements) that are 10–100 times their solar proportions (Lodders & Fegley 1995, 1997b).

Carbon stars are also thought to be responsible for the majority (>95%) of presolar SiC grains (see Daulton et al. 2003). However, the distribution of carbon isotopic compositions of presolar SiC is not at all similar to that of the KFC1 graphite spherules. The ^{12}C/^{13}C distribution for presolar SiC lies mainly within ^{12}C/^{13}C = 30–100, with a maximum in the distribution at 50–60 (Hoppe & Ott 1997; cf. solar ^{12}C/^{13}C = 89), similar to that observed astronomically in the atmospheres of N-type carbon stars (Lambert et al. 1986). A small fraction of SiC ($\sim$5%) grains have ^{12}C/^{13}C ratios <10 and possibly originate from J-type carbon stars. An even smaller fraction ($\sim$1%) originates in SN outflows, based (among other isotopic criteria) on observed excesses of ^{28}Si (which can only be produced in the deep interiors of massive stars; see Zinner 1998; Nittler 2003). The majority of SN SiCs have ^{12}C/^{13}C > 100, up to ratios of several thousand. In comparison, although $\sim$10% of the KFC1 graphites have ^{12}C/^{13}C < 20, there is a prominent gap in the distribution of ^{12}C/^{13}C ratios for graphite that corresponds roughly to the peak in the distribution of AGB SiC, and about two-thirds of the graphites have ^{12}C/^{13}C ratios in the same range as the SiC from SNe.

A question that arises as a result of the isotopic data is whether the KFC1 graphites with isotopically light carbon actually may have originated in SN outflows rather than in AGB atmospheres. Since the advent of high-sensitivity nanometer-scale secondary ion mass spectrometry (NanoSIMS) in recent years, it has become possible to give a fairly definitive answer to this question. With the NanoSIMS one can obtain isotopic data on individual, micrometer-sized presolar grains with little consumption of sample (Stadermann et al. 2005). This isotopic analysis may be followed by diamond ultramicrotome slicing of the grains to produce sections of thickness suitable for TEM analysis ($\leq$100 nm). Finally, the same sections studied in the TEM may be analyzed in the NanoSIMS with sufficient spatial resolution and sensitivity to obtain isotopic data on refractory (nanometer sized) subgrains within the graphite. Using this protocol, Croat et al. (2003) showed that presolar graphite grains from the Murchison meteorite graphite separate KE3 (number weighted mean diameter $\sim$6 μm; 1.65–1.72 g cm^{-3}; Amari et al. 1994), which are identified as originating in SNe on the basis of observed excesses of ^{28}Si and ^{18}O, commonly have internal crystals of TiC. In contrast to KFC1 graphites, however, in SN graphites there are *no* occurrences of carbides enriched in *s*-process transition metal elements (e.g., Zr, Mo, and Ru). On the other hand, NanoSIMS analyses of ultramicrotome slices of KFC1 graphites (Paper I) show that most graphites containing Zr-, Mo-, and Ru-rich carbides really do have isotopically light carbon ($100 < ^{12}\mathrm{C}/^{13}\mathrm{C} < 1000$), a clear indication of formation around late-stage AGB stars, where third dredge-up events transport ^{12}C from 3α He burning as well as *s*-process elements to the stellar surface. Taken together, these observations imply that many of the KFC1 graphites with light carbon *do not* originate in SNe.

Modeling results (Amari et al. 2001) instead suggest that low-metallicity AGB stars can produce light carbon as well as the inferred *s*-process enrichments in Zr, Mo, and Ru needed to condense carbides of these elements. Noble gas isotopic compositions in KFC1 graphites also suggest an AGB origin (Amari et al. 1995). Finally, recent NanoSIMS determinations of Ti isotopic compositions in TiC within KFC1 graphites (Amari et al. 2004) often show excesses in ^{46}Ti and ^{49}Ti relative to ^{48}Ti (with ^{49}Ti/^{48}Ti as high as 5 times the solar ratio), consistent with neutron capture in the He intershell during the third dredge-up in thermally pulsing AGB stars (TP-AGB) with $M \gtrsim 3\ M_\odot$. Therefore, in the treatment that follows, we take (low metallicity) TP-AGB stars as the source of most KFC1 graphites, and base our analyses upon this assumption (see § 4).

3. MASS LIMITS ON STELLAR SOURCES OF PRESOLAR GRAPHITE

In order to derive the combined implications of data on presolar graphite and astronomical observations of carbon stars, it is useful first to determine which members of this class of stars are likely to have contributed to the solar inventory. The most fundamental distinction that can be made is on the basis of stellar mass, since significant mass loss occurs only toward the end of the stellar lifetime. Thus, presolar stars must have evolved beyond the main sequence to have contributed dust to the solar nebula. The lifetime t_* on the main sequence varies in proportion to the mass M_* of the star, and also varies inversely as the power radiated by the star (its luminosity L_*). The

luminosity is, in turn, proportional to M_*^K, where $K = 3.5$ classically. Data from *Hipparcos*, however, suggest that the exponent is better determined as $K = 3.7$ for $M_* \approx 0.5-5\ M_\odot$ (Lampens et al. 1997; Martin et al. 1998). The stellar lifetime t_* is then given in terms of the solar main-sequence lifetime $t_\odot$ as

$$t_* = t_\odot (M_*/M_\odot)^{-2.7}, \quad (1)$$

with $t_\odot \approx 10-11$ Gyr (Iben 1967; Sackmann et al. 1993). The maximum lifetime t_* of stars (corresponding to the minimum mass) that contributed matter to the solar system is then constrained to be approximately the difference between the age of the Galaxy $t_{\rm Galaxy}$ and the age $t_{\rm SS}$ of the solar system, that is, $t_* \lesssim t_{\rm Galaxy} - t_{\rm SS}$. The latter quantity is well determined as $t_{\rm SS} = 4.6$ Gyr, while the former quantity may be estimated from the recent *WMAP* age of the universe (13.7 ± 0.2 Gyr; Bennett et al. 2003). Using these numbers we would find $t_* \lesssim 9.1$ Gyr (and from eq. [1], $M_* \gtrsim 1.04\ M_\odot$).

This t_* is, however, really an extreme upper limit on the lifetime of stars that can contribute to the solar mixture for two reasons. First, $t_{\rm Galaxy}$ is estimated to be less than the age of the universe by $\sim$1 Gyr, based on recent constraints on the age of globular clusters (Krauss & Chaboyer 2003). Second, the limit on t_* implicitly includes the residence lifetime in the ISM of the matter expelled from stars prior to its incorporation in the solar nebula. There are currently no reliable data on the ISM residence lifetimes of presolar grains, but an estimate may be made using theoretical lifetimes of $\lesssim$0.5 Gyr against grain destruction in the ISM (see Jones et al. 1997). With these considerations, we estimate $t_* \lesssim 7.5-8$ Gyr. As equation (1) shows, M_* is relatively insensitive to the uncertainty in the stellar lifetime, varying approximately as the inverse cube root of t_* For t_* in the estimated range, we find $M \gtrsim 1.1\ M_\odot$. We therefore take this as the minimum mass for stars *of any kind* that could have contributed grains to the solar nebula. We also adopt $\sim$1.1 $M_\odot$ as the benchmark for *carbon* stars that could have produced presolar graphite. However, we note that the mass range in which carbon stars are capable of forming is thought to be somewhat more restricted on theoretical grounds, both at low and high mass limits. Gallino et al. (1997) argue that below $\sim$1.3 $M_\odot$, mass loss may cause the stars to undergo too few of the third dredge-up events needed to evolve into carbon stars prior to their evolving into white dwarfs. On the other hand, stars with masses much greater than $\sim$4–5 $M_\odot$ may be subject to hot-bottom burning, which also drastically limits carbon and *s*-process element enrichment. These limits are subject to uncertainties that are difficult to evaluate but broadly consistent with observation.

4. PRESOLAR GRAPHITE AND THE H-R DIAGRAM FOR C STARS

In this section we review the present-day observations of carbon stars, in order to identify among them the possible stellar sources of presolar graphite. Here we make extensive use of the work of Bergeat et al., who derived effective temperatures (Bergeat et al. 2001), luminosities (Bergeat et al. 2002a), and masses (Bergeat et al. 2002b) for a large number ($\sim$300) of carbon stars studied by *Hipparcos* (Perryman 1997). In Figure 1 we present a carbon star H-R diagram adapted from Figure 9 of Bergeat et al. (2002a). Loci of constant stellar radius (in multiples of the solar radius $R_\odot$) are also shown. The carbon stars in Figure 1 are broadly classified as HC (''hot carbon'') stars, CV (''carbon variable'') stars, and Tc (''technetium'') stars. The HC group consists largely of stars that have nonvariable light, but also includes some irregular and small-amplitude variables, carbon Cepheids, and RCrB variables; R stars are mostly included in this group. The CV stars are cool giants that are long-period variable stars (Miras). They include the N stars and the late-stage R stars that can be explained by the third dredge-up. They are close to the tip of the TP-AGB region of the H-R diagram. Bergeat et al. (2002a) further divide the CV stars into seven photometric groups (CV1–CV7). With increasing photometric number, effective stellar temperatures decrease while the stellar mass, luminosity, C/O ratio, and atmospheric opacity increase. The CV stars in groups CV1–CV6 have nearly constant mean surface gravities, with $g = (5.1 \pm 0.7) \times 10^{-3}$ m s^{-2}, or $\log g = -0.3 \pm 0.1$ (cgs). The Tc stars are CV giants that have detectable technetium in their atmospheres, indicating a recent dredge-up of *s*-process material.

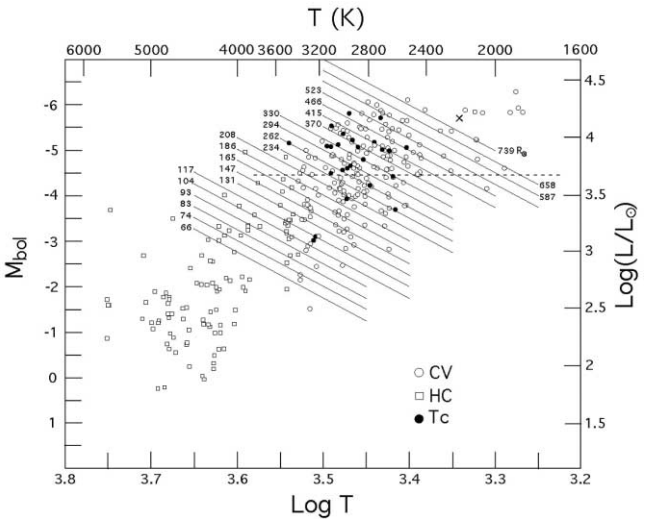

FIG. 1.—Bolometric magnitude ($M_{\rm bol}$) vs. effective temperature (T) for $\sim$300 carbon stars (H-R diagram), adapted from Bergeat et al. (2002a). CV = variable carbon giants, HC = hot carbon stars, Tc = variable carbon giants with detectable technetium. Loci of constant stellar radius (in terms of the solar radius $R_\odot$) are indicated. The dashed horizontal line at 4700 $L_\odot$ corresponds to carbon stars with $M = 1.1\ M_\odot$, the minimum mass needed for a star to have evolved sufficiently rapidly to have contributed grains to the solar nebula. The closest and best-studied CV star IRC +10216 is shown as the x-symbol. See text for discussion.

Bergeat et al. (2002b) derived average stellar masses for each of the seven photometric groups. They found that for groups CV2–CV5 (1–3 $M_\odot$ range) the mean luminosity L is correlated with mean group stellar mass M as $\log(L/L_\odot) = (0.497 \pm 0.075) \log(M/M_\odot) + (3.66 \pm 0.03)$. From this it appears that the luminosity of CV stars approximately follows the mass dependence $L \propto M^{1/2}$ (as compared to the main-sequence mass-luminosity relation $L \propto M^{3.7}$). In the present work we also explicitly consider more massive stars, and if we use the Bergeat et al. (2002b) data in the 1–8 $M_\odot$ range we can parameterize the mass-luminosity relation as

$$\log(L/L_\odot) = 0.604 \log(M/M_\odot) + 3.65. \quad (2)$$

This relation has uncertainties comparable to and gives nearly identical results as the Bergeat et al. (2002b) relation for groups CV2–CV5, but also yields a mass in somewhat better agreement with the mean mass of members of the CV7 group ($\sim$8 $M_\odot$). We therefore adopt this mass-luminosity relation for all stellar masses of interest here.

Regardless of which relation one uses, the lower limit of 1.1 $M_\odot$ on the mass of stars that contributed grains to the solar

nebula (§ 3) implies a minimum carbon star luminosity $L_* \sim 4700\ L_\odot$ ($M_{\rm bol} = -4.46$). This luminosity threshold is shown as a dashed horizontal line in Figure 1. It can be seen that this threshold excludes all but two of the HC stars, effectively eliminating stars of this group as potential contributors of presolar grains. We thus reach our first principal conclusion, that CV stars of $M \gtrsim 1.1\ M_\odot$ are the likely source of KFC1 graphite grains having enhancements of *s*-process elements.

From a comparison of theoretical tracks of TP-AGB stars with the empirical mass-luminosity relationship for CV stars, Bergeat et al. (2002b) conclude that, on average, the CV data are characteristic of the TP-AGB phase. The data are also consistent with carbon star metallicities that are less than the solar metallicity. As noted above (§ 2), isotopic compositions of noble gases and Ti in KFC1 graphites are consistent with these same conditions, lending further support to the idea that CV stars are the likely stellar source.

5. ASTROPHYSICAL INFERENCES FROM EQUILIBRIUM THERMODYNAMICS

Further constraints on the conditions in circumstellar envelopes come from the application of equilibrium thermodynamics to the chemical composition of presolar grains. For example, Lodders & Fegley (1997a) noted that the pattern of trace element enrichment in "mainstream" presolar SiC is exactly mirrored in the elemental depletion patterns observed astronomically in the atmospheres of N-type carbon stars. They showed that these depletion patterns are consistent with the trace element partitioning into condensing SiC predicted by equilibrium thermodynamics. We take this agreement to indicate that equilibrium condensation thermodynamics provides a reliable guide to the composition of condensates in AGB outflows. As another example, TiC crystals (usually in solid solution with refractory elements such as Mo and Zr) are often observed within KFC1 graphite spherules. They are found in $\gtrsim \frac{1}{6}$ of well-graphitized spherules, and in nearly half of these instances at the spherule centers (Paper I; Bernatowicz et al. 1996). The clear implications are that TiC condensation preceded that of graphite and that TiC crystals sometimes served as heterogeneous nucleation centers for the growth of graphite. As we demonstrate below, the application of equilibrium thermodynamics to these observations allows quantitative inferences to be drawn about temperatures, pressures, and C/O ratios in the grain condensation environment. These inferences can be checked against astronomical observation and can also be used to inform kinetics calculations of grain growth.

Figure 2 displays condensation temperatures for graphite and TiC as a function of the gas pressure and C/O ratio, under conditions of thermodynamic equilibrium. Only ratios C/O > 1 are shown, because at lower values all C is tied up in the very stable CO molecule in the gas phase; it is only when the C number density exceeds that of O that sufficient "free carbon" (in the form of C_2H_2) is available to form graphite and carbides (see Lodders & Fegley 1995; Sharp & Wasserburg 1995). Figure 2 assumes that H is the dominant gas in determining the total ambient pressure. Dredge-ups enhance C but not O, so that the O/H ratio remains unchanged. Thus, the pressure abscissa can be used without ambiguity, even though it is the "free carbon" pressure that controls the condensation sequence of carbon-bearing solid phases.

Inspection of Figure 2 shows that the graphite condensation temperature is relatively insensitive to pressure but strongly dependent on C/O, while the TiC condensation temperature depends on pressure but is insensitive to C/O. The fact that the condensation curves cross means that whether TiC will start forming before or after graphite depends on the ambient pressure. The higher the C/O ratio, the greater is the pressure required for TiC to condense before graphite.

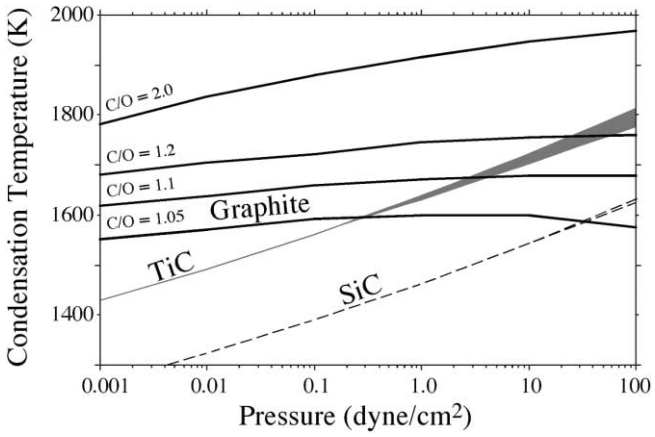

FIG. 2.—Equilibrium condensation temperatures for graphite, titanium carbide (TiC), and silicon carbide (SiC) as a function of total pressure and C/O ratio (from 1.05 to 2.0). The Ti/O and Si/O ratios are assumed to be solar. The TiC and SiC condensation temperatures, displayed as envelopes, are for C/O $\geq$ 1.05. Data are from Lodders & Fegley (1995). See text for discussion.

For example, condensation of TiC before graphite will occur at $P \gtrsim 0.3$ dynes cm^{-2} for C/O $= 1.05$, at $P \gtrsim 3$ dynes cm^{-2} for C/O $= 1.1$, and $P \gtrsim 30$ dynes cm^{-2} for C/O $= 1.2$. However, the C/O ratio cannot be increased much beyond this if TiC is to condense before graphite. As C/O approaches $\sim$1.5 the required pressure reaches photospheric values for the AGB stars considered here ($\sim$700–1400 dyne cm^{-2}; see Soker & Harpaz 1999), and at the photosphere the temperature is far too high for any grains to condense. Instead, the grains must condense at radii greater than the photospheric radius where both temperatures and pressures are much lower. So the presolar graphites with nuclei of TiC observed in KFC1 certainly indicate $1 \lesssim$ C/O $\lesssim 1.2$ in the circumstellar atmospheres where they formed, as originally argued by Sharp & Wasserburg (1995).

This conclusion is robust, and moreover is consistent with astronomical observations of AGB stars. Using the C/O ratios determined by Lambert et al. (1986), Bergeat et al. (2001) calculated the mean C/O for each CV photometric group, which progressively increases from C/O $= 1.04 \pm 0.02$ for group CV2 to C/O $= 1.25 \pm 0.27$ for group CV6, with a mean over all groups of C/O $= 1.15 \pm 0.16$. These astronomical C/O ratios compare favorably with the constraints on C/O derived from presolar graphite. We note in passing that no interesting limit on C/O, other than C/O > 1, can be derived from the observations of KFC1 graphites in which no internal crystals of TiC and/or other carbides are detected.

The plausibility of the C/O ratios inferred from the assumption of thermal equilibrium condensation means that confidence can be placed in correlated physical inferences about the circumstellar environments in which the graphite grains formed. One important inference is in regard to the mass-loss rate for CV stars. Keeping in mind the possibility of anisotropy of the gas and dust moving in a stellar outflow with a radial velocity $v(\boldsymbol{R}) \equiv v(R, \theta, \phi)$ in the region of dust formation, the mass-loss rate $\dot{M}$ is given by the continuity relation

$$\dot{M} = \int_0^{\pi} \int_0^{2\pi} \rho(R, \theta, \phi) v(R, \theta, \phi) R^2 \sin\theta \, d\theta \, d\phi, \quad (3a)$$

where the density $\rho(\boldsymbol{R}) \equiv \rho(R, \theta, \phi)$ at location $\boldsymbol{R}$ [shown explicitly above in spherical coordinates as (R, θ, ϕ)] is related to the pressure $P(\boldsymbol{R})$ at that location by

$$\rho(R, \theta, \phi) = \frac{\mu P(R, \theta, \phi)}{kT(R, \theta, \phi)N_{\rm A}}. \quad (3b)$$

Here μ is the molecular weight of the gas, R is the grain formation radius measured from the star's center, k is Boltzmann's constant, $N_{\rm A}$ is Avogadro's number, and T is absolute gas temperature. Under the special condition of spherical symmetry of the outflow, equation (3a) reduces to the standard form

$$\dot{M} = 4\pi R^2 \rho(R) v(R). \quad (3c)$$

For solar composition gas at $T \sim 1700$ K (see Fig. 2) we use $\mu = 2.34$ g mol^{-1}. As noted above, C/O ~ 1.1 for CV stars requires that the pressure $P \gtrsim 3$ dynes cm^{-2} in the stellar atmosphere for TiC to condense before graphite. Even if the outflow speed v in the grain formation region is only 1/10 of a typical terminal outflow speed of $\sim$15 km s^{-1} for AGB stars and the grains begin to condense at $R \sim 3$ AU (see § 6), equations (3a)–(3c) yield $\dot{M} \sim 3 \times 10^{-3}\ M_\odot$ yr^{-1}.

This estimate is an order of magnitude larger than the greatest mass-loss rates observed for AGB stars (see below). This reiterates a conclusion of Bernatowicz et al. (1996): if KFC1 presolar graphites form in AGB atmospheres, then they must form in density concentrations (such as clumps or jets) in the mass outflow; otherwise the equilibrium condensation pressures imply mass-loss rates that are too large to be consistent with anything close to a spherically symmetric outflow.

In § 7 we show that this conclusion follows as well from considerations of growth kinetics as applied to the observed sizes of KFC1 graphite grains and their internal carbides. In the following section (§ 6), however, we consider several semiempirical relationships that are informed by the equilibrium thermodynamics and are independent of considerations of grain size, in order to make quantitative estimates of the radii at which such grains form, the mass outflow speeds at these radii, and the duration of grain growth.

6. THE CIRCUMSTELLAR GRAPHITE FORMATION ENVIRONMENT: RADII, OUTFLOW SPEEDS, AND DURATION OF GRAIN GROWTH

The dynamics of mass loss is closely correlated with dust formation in the atmospheres of evolved stars. In AGB stars the periodic pulsation enhances the gas density through shocks in the stellar atmosphere above the photosphere, promoting the condensation of dust grains (Bowen 1988). Copious mass outflow occurs largely because grains are coupled to the radiation field of the star, which accelerates them by radiation pressure; momentum is in turn transferred to gas molecules by collisions with grains. The dust/gas mixture is effectively a two-component fluid whose motion and the atmosphere structure are dynamically coupled and have to be determined self-consistently. In particular, the radiation pressure on the grains determines the velocity field of the outflow and thus the density distribution, while the density distribution itself determines the conditions of radiative transfer within the outflow and thus the effective radiation pressure. Here we will not deal with this difficult problem, but instead we will rely on parameterizations of the results from detailed dynamical studies (Netzer & Elitzur 1993; Habing et al. 1994; Ivezic et al. 1998; Winters et al. 2000).

A brief outline of our analytical strategy in this section is as follows. We enter the masses (§ 3) and temperatures and luminosities (§ 4) of carbon stars capable of producing presolar graphite into a mass-loss rate formula based on dynamical wind models to infer $\dot{M}$ for these stars. We assume initially, for the sake of simplicity, that mass outflows from AGB stars are spherically symmetric. (As we will see, the comparison of model results with inferences from presolar grain data [§ 7] will force us ultimately to discard this assumption, and to conclude instead that the density structure of the outflows is neither smooth nor symmetric. However, we note here that the conclusions reached in this section will remain unaffected as long as the mass outflow velocities are radial.) We also derive an approximate relationship $R(T)$ between radial distances R and local temperatures T for a given luminosity. The temperature range ΔT from the point of initial condensation to effective quenching of growth (suggested by equilibrium thermodynamics and kinetics) then yields a plausible radial interval ΔR for grain growth. We use the observed astronomical relationship between terminal outflow velocity v_e and $\dot{M}$, along with parameterized results of dynamical calculations, to characterize the outflow velocity field $v(R)$ from the condensation radius outward as a function of dust optical depth. Integration of $dR/v(R)$ over radial interval ΔR then gives a numerical estimate for the time interval Δt over which solid condensates could grow.

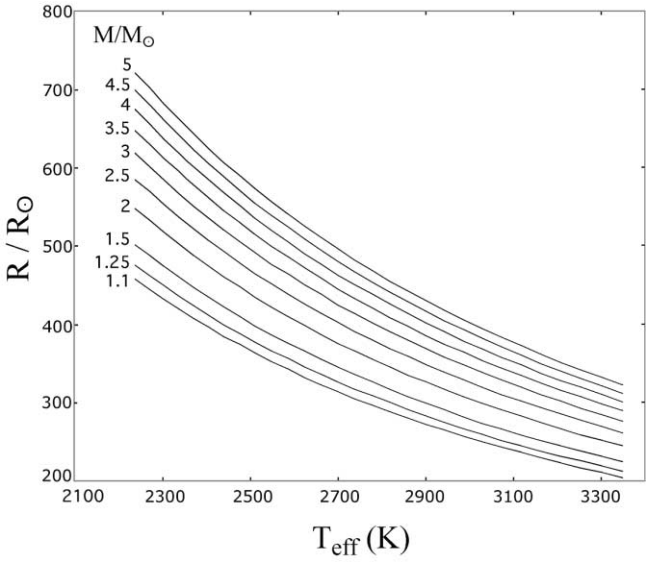

FIG. 3.—Stellar radii R (expressed as multiples of the solar radius) as a function of effective temperature $T_{\rm eff}$ for CV stars with masses from 1.1 to 5 $M_\odot$. See text for discussion.

The lower limit on the mass of carbon stars that are capable of contributing presolar graphite to the solar nebula restricts our considerations to stars with effective temperatures from $T_{\rm eff} \sim$ 1900 to 3400 K, luminosities from $L \sim 4700$ to 19,500 $L_\odot$, and radii from $R \sim 200$ to 1300 $R_\odot$, as may be noted from inspection of Figure 1. A comparatively small number of stars, namely very cool, highly luminous ones (including the well-studied carbon star IRC +10216, with a very large mass-loss rate), populate one extreme edge of this range. We will consider this subset separately in a later discussion and restrict ourselves here to the most densely populated portions of this region of the H-R diagram. In particular, we investigated stellar masses from $M = 1.1$ to 5 $M_\odot$ and temperatures from $T_{\rm eff} = 2240$ to 3350 K. The selected mass range translates into luminosities from 4700 to 11,700 $L_\odot$, using the mass-luminosity relation for CV stars discussed in § 4.

Carbon stars in the selected mass range are shown in Figure 3, a plot of stellar radius R (in solar radii) against effective

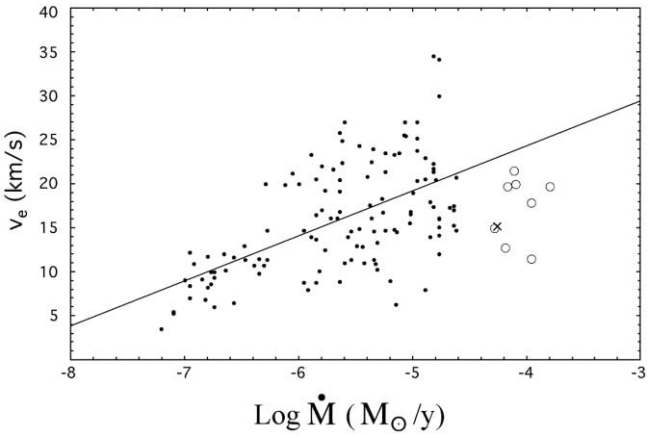

FIG. 4.—Mass outflow terminal velocity v_e as a function of mass-loss rate for 132 carbon stars (from data compiled by Netzer & Elitzur 1993). The CV star IRC +10216 is also shown (x-symbol). A linear least-squares fit to the data represented as dots (123 stars) is also displayed. Mass-loss rates greater than $2.5\times10^{-5}\ M_\odot\ \mathrm{yr}^{-1}$ are shown as open symbols and are not included in the fit. See text for discussion.

temperature $T_{\rm eff}$. It is seen that the stellar radii range from $R\sim$ 450 to 500 $R_\odot$ for the cooler low-mass (1.1–1.5 $M_\odot$) stars to $R\sim700\ R_\odot$ for the cooler intermediate-mass (4–5 $M_\odot$) stars, and from $R\sim200$ to 320 $R_\odot$ for the hotter stars over the entire mass range. All of these stars are giants, as can be appreciated from noting that the radii of even the smallest are about 1 AU (215 $R_\odot$).

Because the allowable time interval Δt over which grains can nucleate and grow is intimately tied to the outflow velocity v and thence to the mass-loss rate $\dot{M}$ (eq. [4]), we need first to estimate $\dot{M}$ for the stars of interest. Arndt et al. (1997) provide a parameterized $\dot{M}$ from dynamical studies in terms of six variables: the stellar temperature, mass, luminosity, C/O ratio, pulsation period, and pulsation amplitude. As discussed by these authors, $\dot{M}$ is only weakly dependent on the last three quantities, so it is possible to estimate the mass loss in terms of only the first three without much loss of accuracy.

We use their mass-loss rate formulation in terms of only T, M, and L in calculations described below. The $\dot{M}$ dependence on these parameters is given by Arndt et al. (1997) as

$$\log\dot{M} = -4.93 - 8.26\log\left[\frac{T(\mathrm{K})}{2600}\right] + 1.53\log\left(\frac{L/L_\odot}{10^4}\right) - 2.88\log\left(\frac{M}{M_\odot}\right). \quad (4)$$

It can be seen that $\dot{M}$ is most strongly dependent on T. It increases with increasing L but decreases with increasing T and M. These functional dependences are fully consistent with the observations (e.g., Schöier & Olofsson 2001). It is important to note, however, in the present context that these variables are not all independent, because M and L are coupled through the mass-luminosity relation for CV stars (eq. [2], § 4).

We note that some of the masses we consider here (see Fig. 3) are greater than the upper mass limit ($\sim2\ M_\odot$) of the model grid of Arndt et al. (1997), but only minor changes in the values of the coefficients of equation (4) are expected. Indeed, the mass-loss rates predicted by equation (4) for the stellar masses, effective temperatures, and luminosities considered here lie entirely within the range of the observed values for carbon stars (Fig. 4). Moreover, the predicted maximum $\dot{M}$ of several times $10^{-5}\ M_\odot\ \mathrm{yr}^{-1}$ for these stars is consistent with the observed maximum, with the exception of a few carbon stars whose mass outflows are likely inhomogeneous (see below).

We now consider observational evidence relating mass outflow velocity to mass-loss rate. In Figure 4 we plot terminal outflow velocities v_e as a function of $\dot{M}$ for 132 carbon stars based on a compilation by Netzer & Elitzur (1993). Stars with $\dot{M} < 2.5\times10^{-5}\ M_\odot\ \mathrm{yr}^{-1}$ are represented by dots, and stars with mass-loss rates greater than this are shown as open circles. In the first group, there is a distinct trend of increasing terminal velocity with increasing mass-loss rate. We display a linear fit to the first group of data, and it can be seen that terminal velocities from the second group all lie below this trend. Netzer & Elitzur (1993) attribute this falloff in v_e at high mass-loss rates for carbon stars to a progressively steeper decline in mean opacity with distance from the star as $\dot{M}$ increases. The equation for the fitted line is

$$v_e = (5.11\pm0.65)\log\dot{M} + (44.8\pm3.7)\ \mathrm{km\ s^{-1}}, \quad (5)$$

with a standard deviation about the line of $\pm5.12\ \mathrm{km\ s^{-1}}$. Thus, even though the trend is significant, the scatter is considerable. This is not unexpected, even aside from observational uncertainties. For example, Habing et al. (1994) point out that the stellar luminosity and the dust-to-gas ratio in the outflow ($\sim2.5\times10^{-3}$ by mass for carbon stars; Ivezic et al. 1998) influence v_e so that greater values for either of these lead to increased terminal outflow velocities. They also speculate that the dust-to-gas ratio may depend on luminosity. If so, then there is the possibility that even the factor of $\sim$2–3 variations in pulsation luminosity that occur in CV stars (Feast et al. 1982; Bergeat & Sibai 1983; Hofmann et al. 1998) may change this ratio, leading to variations in v_e. We will explicitly consider the consequences of such luminosity variations on grain growth times and grain diameters below. For the present analysis, we will consider the fit represented by equation (5) to give a reasonable approximation of the average dependence of v_e on $\dot{M}$, and we will use this relationship hereafter. We will also consider the consequences of the dispersion of v_e values in our calculations of the grain growth time interval Δt.

We note that the stars in Figure 4 with $\dot{M} > 2.5\times10^{-5}\ M_\odot\ \mathrm{yr}^{-1}$ appear to constitute a distinct group. One of their members is the well-studied (nearest) CV star IRC +10216 (see Jura 1994). Weigelt et al. (1998), using speckle-masking interferometry, show that the mass outflow from this star is not spherically symmetric nor homogeneous, but is highly fragmented. They conclude that IRC +10216 appears to be in a very advanced stage of its AGB evolution, perhaps in a phase immediately preceding its departure from the AGB. If the same is true for the other stars in this group (Fig. 4), then their inhomogeneous mass loss violates an implicit premise of our present analysis, and so we will consider them separately later.

Now consider a grain of surface area A that is irradiated by the star over approximately half of its surface, and in turn radiates from its entire surface. At equilibrium, the input power and radiated power are the same, so $LA/(8\pi R^2) = A\sigma T_G^4$, where L is the stellar luminosity, R is radial distance relative to the star's center, T_G is the grain temperature, and the Stefan-Boltzmann constant is $\sigma = 5.6705\times10^{-8}\ \mathrm{W\ m^{-2}\ K^{-4}}$. This gives $R^2 = L/(8\pi\sigma T_G^4)$.

In order to establish a convenient reference length scale R_0, we normalize with $T_0 = 1000$ K and $L_0 = L_\odot = 3.846\times10^{26}$ W (see Ivezic et al. 1998). We obtain $R_0 = 23.6\ R_\odot$, using

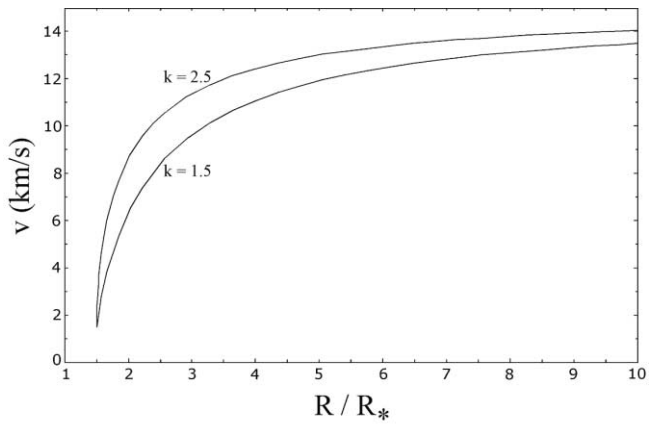

FIG. 5.—Mass outflow velocity $v(R)$ as a function of radius R from eq. (7), for the case in which the terminal velocity $v_e = 15$ km s^{-1}, $R_{\rm cond}/R_* = 1.5$, and $\epsilon = 0.1$. The velocity field is shown for optically thin ($k = 1.5$) and for optically thick outflows ($k = 2.5$). See text for discussion.

the solar radius $R_\odot = 6.961 \times 10^8$ m. In terms of this length scale, we write $R = R(L, T)$ as

$$\frac{R}{R_\odot} = 23.6 \left(\frac{L}{L_\odot}\right)^{1/2} \left(\frac{1000\ \mathrm{K}}{T_G}\right)^2. \quad (6)$$

If we can now find a relation between radial position and outflow velocity, then we can use equation (6) to find outflow velocities within a given temperature range.

To do this, we make use of parameterizations of detailed dynamical models for the outflow velocity field given by Ivezic et al. (1998). As noted previously, it is the coupling of the stellar radiation field to the grains that drives the mass outflow, so the velocity field depends on the radius $R_{\rm cond}$ where grains first condense, as well as on the velocity of the atmosphere at this radius. Defining $\epsilon = v_{\rm cond}/v_{\rm e}$ as the ratio of the outflow velocity $v_{\rm cond}$ at the grain condensation radius to the terminal velocity v_e, the velocity field $v(R)$ at radius R is well characterized by

$$v(R) = v_e \left[\epsilon^k + \left(1 - \epsilon^k\right)\left(1 - \frac{R_{\rm cond}}{R}\right)\right]^{1/k}. \quad (7)$$

The dependence of $v(R)$ on stellar mass and ϵ is practically negligible (Ivezic et al. 1998). In the analysis, we formally take $\epsilon = 0.1$. In practice, $v(R)$ is so insensitive to small ϵ that if we simply take $\epsilon = 0$ it makes no difference in the velocity field for any R moderately greater than $R_{\rm cond}$. In that case, $v(R) = v_e(1 - R_{\rm cond}/R)^{1/k}$. The power index k has a weak dependence on the dust optical depth, ranging from $k = 1.5$ in optically thin outflows to $k = 2.5$ in optically thick outflows. We assume that this range in k brackets the physical situations of interest here.

In Figure 5 we illustrate $v(R)$ for the specific case where $v_e = 15$ km s^{-1}, $\epsilon = 0.1$, and the condensation of grains begins at $R = 1.5\ R_*$, where R_* is the stellar radius. The effect of k on $v(R)$ is evident. For all radii $R > R_{\rm cond}$, the velocity is greater for higher dust opacity ($k = 2.5$). While the $v(R)$ are similar at radial distances many times the stellar radius, they are significantly different at smaller radii near $R_{\rm cond}$. This means that, for a given stellar luminosity and effective temperature, the time available for the growth of dust in the outflow is greater in optically thin envelopes, as we discuss below. It is also evident that for all k the velocity gradient near $R_{\rm cond}$ is large. Thus, whether grains form nearly at rest ($\epsilon \sim 0$) or at 1/10 the terminal velocity ($\epsilon \sim 0.1$) matters little, because they are accelerated to much greater velocities after only modest radial displacement.

We turn our attention to the temperature range ΔT_G over which grains can condense and grow. Inspection of Figure 2 shows that for the inferred range $1 \lesssim$ C/O $\lesssim 1.2$ for CV stars that can form circumstellar graphite and TiC (§ 4), a plausible upper limit on the temperature of grain condensation is $\sim$1800 K. The choice of a temperature at which graphite and TiC growth have effectively ceased may be estimated from both equilibrium thermodynamics and kinetics. Considering equilibrium thermodynamics first, for C/O in the above range, as the temperature drops graphite will react with gaseous Si to form SiC, and graphite will not tend to form once SiC begins to appear (Sharp & Wasserburg 1995). The SiC condensation temperatures closely parallel those for TiC (Fig. 2), at temperatures about 175 K lower than for TiC (Lodders & Fegley 1995), implying effective cessation of graphite growth by $T_G \sim 1200$ K for any plausible pressure. Turning to kinetics, we note that the continuity relation for $\dot{M}$ (eqs. [3a]–[3c]) implies that the ratio of gas pressures $P_{1800\,\rm K}/P_{1200\,\rm K} = (R_{1200\,\rm K}/R_{1800\,\rm K})^2(v_{1200\,\rm K}/v_{1800\,\rm K})$(1800 K/1200 K). According to equation (6), for a given luminosity the first term is $(1800/1200)^4 \sim 5$. Assuming that the velocity at which grains condense is $\sim 0.1 v_e$, the velocity at 1200 K will be roughly 10 times the velocity at condensation, i.e., $v_{1200\,\rm K}/v_{1800\,\rm K} \sim 10$. Thus, $P_{1800\,\rm K}/P_{1200\,\rm K} \sim 75$. Since the rate of grain growth (see § 7) is proportional to pressure, it will also drop by a factor of $\sim$75. When the temperature reaches 1000 K, the pressure and grain growth rate will each have decreased by a factor of $\sim$190 below their values at 1800 K. From consideration of both equilibrium thermodynamics and kinetics, we therefore adopt the temperature $T_G = 1000$ K as a conservative estimate of the temperature at which circumstellar graphite growth effectively ceases. The adopted temperature range from 1800 to 1000 K is also sufficiently broad so as to compass any plausible temperature differences between dust grains and gas during grain growth, particularly at the low-temperature end of the range.

In Table 1 we list the radial distances calculated from equation (6) that correspond to the estimated growth temperature interval ΔT_G from 1800 to 1000 K, for the range of stellar masses and luminosities investigated. Because of the weak dependence of R on L, there is only a spread of $\sim$1.4 AU in the initial condensation radius (R at 1800 K) over the entire (1.1–5 $M_\odot$) stellar mass range, with the mean distance $R_{1800\,\rm K} = 3 \pm 0.7$ AU.

TABLE 1

CIRCUMSTELLAR GRAPHITE CONDENSATION AND GROWTH RADII

M		L	$R_{1800\,\rm K}$		$R_{1000\,\rm K}$		ΔR
($M_\odot$)	$M_{\rm bol}$	($L_\odot$)	AU	$R_\odot$	AU	$R_\odot$	(AU)
1.1.....	−4.46	4700	2.32	499	7.53	1620	5.21
1.25.....	−4.54	5080	2.42	520	7.83	1680	5.41
1.5.....	−4.66	5670	2.55	548	8.27	1780	5.72
2.0.....	−4.85	6750	2.78	597	9.02	1940	6.24
2.5.....	−4.99	7720	2.98	640	9.65	2070	6.67
3.0.....	−5.11	8620	3.15	677	10.2	2190	7.05
3.5.....	−5.21	9460	3.30	709	10.7	2300	7.38
4.0.....	−5.30	10250	3.43	737	11.1	2390	7.69
4.5.....	−5.38	11000	3.56	765	11.5	2470	7.97
5.0.....	−5.45	11700	3.67	789	11.9	2560	8.22

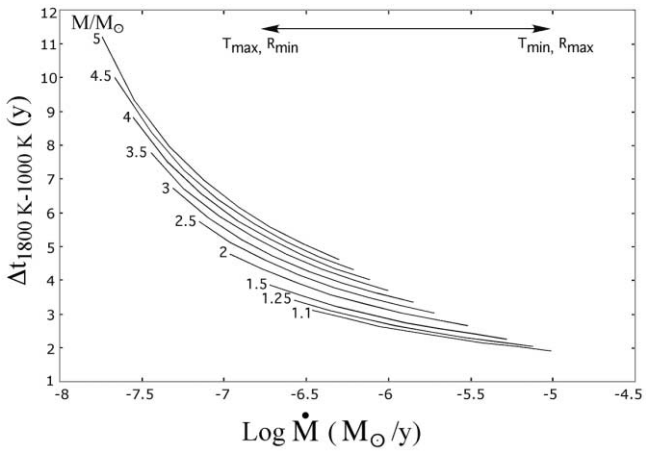

FIG. 6.—Maximum graphite growth intervals in AGB carbon star atmospheres in the temperature range $T = 1800-1000$ K, as a function of stellar mass and mass-loss rate. For a given stellar mass, the left end of the curve corresponds to the maximum effective temperature (3350 K) and minimum photospheric radius shown in Fig. 3, and the right end corresponds to the minimum effective temperature (2240 K) and maximum photospheric radius in that figure. The power index $k = 2.5$ (optically thick outflow) in eq. (7) was used. See text for discussion.

Using the condensation radii at 1800 K ($R_{\rm cond} = R_{1800\,\rm K}$) in Table 1 and $v(R)$ from equation (7), the allowed interval Δt between the onset of grain growth at 1800 K and its cessation at 1000 K may be estimated as

$$\Delta t = \int_{R_{1800\,\rm K}}^{R_{1000\,\rm K}} \frac{dR}{v(R)}. \qquad (8)$$

Because of the conservative limits on the temperature range ΔT_G, as discussed above, the grain growth intervals Δt calculated from equation (8) represent upper limits on the time during which graphite and TiC condensates can grow in AGB atmospheres.

Figure 6 displays results for equation (8) using the integration limits from Table 1 and assuming an optically thick outflow ($k = 2.5$ in eq. [7]). In an optically thin outflow ($k = 1.5$ in eq. [7]), the time intervals displayed in Figure 6 are increased by a factor of 1.26. The grain growth interval Δt, operationally defined here as the time required for the temperature of a parcel of gas in the outflow to cool from a condensation temperature of 1800 K to 1000 K, increases systematically with stellar mass. For the entire stellar mass range considered, Δt varies by about an order of magnitude, roughly from 2 to 10 yr. The growth intervals Δt are minimal for the smallest possible stellar mass ($1.1\ M_\odot$) that could contribute circumstellar graphite to the solar nebula (§ 3). Overall, the growth of circumstellar graphite grains is constrained to occur in the relatively short time interval of a few years, as opposed to far longer time intervals that might have been deduced from kinetics and/or considerations of grain size (as discussed below in § 7).

For any stellar mass, the interval Δt available for grain growth is the smallest for the largest mass-loss rate. As inspection of Figure 6 shows, Δt increases with effective stellar temperature $T_{\rm eff}$, and more steeply so for larger stellar masses. For example, with $M = 1.1\ M_\odot$, Δt increases by 1.2 yr from $T_{\rm eff} = 2240$ to 3350 K, but for $M = 5\ M_\odot$ it increases by 6.6 yr in the same temperature range. The decreases in $\dot{M}$ and v_e with increasing $T_{\rm eff}$ (eqs. [4] and [5]) cause a rapid increase in Δt as M increases.

Up to this point, we have set aside the important consideration that the carbon stars that are producers of presolar graphite are *variable* (CV) stars, meaning that their luminosities, effective temperatures, and radii vary periodically with time. We now explore the implications for the foregoing discussion if this variability is taken into account. For the Bergeat et al. (2002b) photometric groups (CV2–CV7) that are of interest in the present context, the mean fundamental pulsation period is about 1 ± 0.4 yr.

Within these photometric groups, the luminosities range from a minimum luminosity $L_{\rm min} = (0.56 \pm 0.05)L_{\rm nom}$ to a maximum luminosity $L_{\rm max} = (2.35 \pm 0.30)L_{\rm nom}$, where $L_{\rm nom}$ is the nominal (mean) luminosity (Bergeat et al. 2002a). Much of this range in luminosity ($L_{\rm max}-L_{\rm min}$) is attributable to variation of stellar luminosity during pulsation. For example, several studies (Feast et al. 1982; Bergeat & Sibai 1983) have shown that carbon Miras have luminosity amplitudes of up to $\sim$1.2 mag in $M_{\rm bol}$ (i.e., $L_{\rm max}/L_{\rm min} \sim 3$), as compared to $L_{\rm max}/L_{\rm min} \sim 4$ within the CV photometric groups. In the following, we thus take the photometric group luminosity range to be a good estimate of the maximum luminosity variation expected for any given CV star. We also assume that a photospheric temperature $T_{\rm eff} + 200$ K at minimum luminosity and radius and $T_{\rm eff} - 200$ K at maximum luminosity and radius are representative of the variation of $T_{\rm eff}$ during thermal pulsation (Bergeat & Sibai 1983; Bessell et al. 1996).

In Figure 7 we display outflow velocities $v(R)$ for minimum, nominal, and maximum luminosity of a $1.25\ M_\odot$ star with nominal $T_{\rm eff} = 2510$ K and $L_{\rm nom} = 5080\ L_\odot$, whose photospheric temperature varies as indicated above. Time intervals, in decrements of 100 K, from 1800 to 1000 K are shown as dots on the $v(R)$ curves, and the positions of the photosphere for the various luminosities are shown as arrows. The time interval Δt between 1800 and 1000 K varies as the luminosity changes (from 2.2 to 2.8 yr). The luminosity also changes R(1000 K) by a factor $\sim$2 from $L_{\rm min}$ to $L_{\rm max}$. The substantial increase in v(1000 K) from $L_{\rm min}$ to $L_{\rm max}$ is mainly due to the variation in photospheric temperature, to which $\dot{M}$ and $v(R)$ are quite sensitive (eqs. [4], [5], and [7]). At $L_{\rm max}$, the mass-loss rates are maximal, reaching

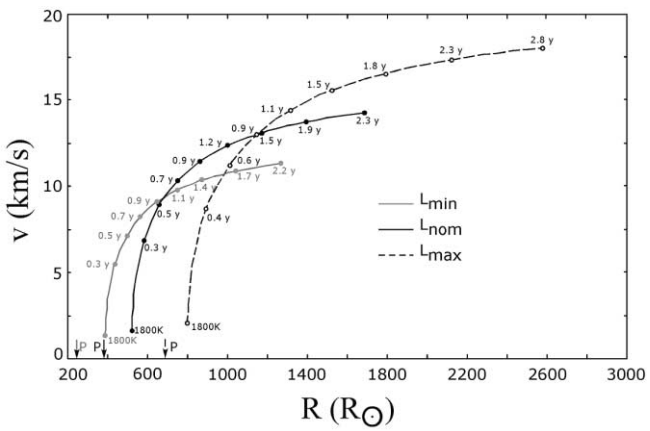

FIG. 7.—Outflow velocity as a function of radius for a CV star with mass $M = 1.25\ M_\odot$, $T_{\rm eff} = 2510$ K, nominal luminosity (*solid curve*) $L_{\rm nom} = 5080\ L_\odot$, and nominal radius $R_{\rm nom} = 377\ R_\odot$. Circles on curves are markers for 100 K decrements in grain temperature to 1000 K, starting at 1800 K. Times (in years) elapsed from 1800 K are shown next to these temperature markers. The power index $k = 2.5$ (optically thick outflow) in eq. (7) was used in calculating $v(R)$. Velocity profiles for $L_{\rm min} = 0.56L_{\rm nom}$ and for $L_{\rm max} = 2.35L_{\rm nom}$ are also shown. It is assumed that for $L_{\rm min}$, $T = T_{\rm eff} + 200$ K, and that for $L_{\rm max}$, $T = T_{\rm eff} - 200$ K. The arrows marked with a "P" show the position of the photosphere for the different luminosities. See text for discussion.

$\dot{M} = 7.8\times10^{-5}$, 1.5×10^{-5}, and 4.0×10^{-6} $M_\odot$ yr^{-1} for stars of 1.1, 2.5, and 5 $M_\odot$, respectively (see Fig. 6).

Inspection of Figure 7 shows that the velocity gradient is qualitatively constant for $\Delta t \lesssim 0.3$ yr ($\Delta T \sim -100$ K) and that it is also qualitatively the same for $L_{\rm min}$, $L_{\rm nom}$, and $L_{\rm max}$. Thus, assuming a fundamental pulsation period of approximately 1 yr, in the quarter-period that the luminosity increases from $L_{\rm min}$ to $L_{\rm nom}$ the velocity gradient will not have changed significantly. This means that the radial distance traversed by grains that formed at 1800 K and that $L_{\rm min}$ will not be much affected by the increase of luminosity to $L_{\rm nom}$. However, inspection of Figure 7 shows that when $L = L_{\rm nom}$, the radial distance between the grains and the advancing photosphere is less than it was at the time that the grains formed. The fact that the grains are between the $L_{\rm nom}$ photosphere and the 1800 K radius at $L_{\rm nom}$ means that the grains will be heated to a temperature significantly above 1800 K and thus will probably evaporate. The overall effect, then, will be to delay permanent grain formation until the luminosity is near $L_{\rm max}$ and to make the effective grain formation interval Δt a value more characteristic of $L_{\rm max}$ than of $L_{\rm nom}$. Grains forming near $L_{\rm max}$ will not be heated above their initial formation temperature by the thermal pulsation cycle and will survive. Some grains that form between $L_{\rm min}$ and $L_{\rm max}$ will thus be subject to conditions at neither extreme of evaporation or persistent cooling; i.e., they will be reheated.

For all stellar masses and effective temperatures considered here, the situation described above persists, although with some differences in the details. As noted previously, the outflow velocities decrease with increasing stellar mass, leading to longer growth time intervals Δt (Fig. 6). These time intervals are only weakly dependent on luminosity. For the smallest stellar mass considered (1.1 $M_\odot$), Δt is only 23%–33% larger at $L_{\rm max}$ than at $L_{\rm nom}$ (for both $k = 1.5$ and 2.5) over the entire effective temperature range (3350–2240 K). For the largest stellar mass considered (5 $M_\odot$), Δt is 0%–24% larger at $L_{\rm max}$ than at $L_{\rm nom}$ over this temperature range. Lastly, at higher effective temperatures ($T_{\rm eff} > 3100$ K) and (only) for larger stellar masses ($M \gtrsim 2.5$ $M_\odot$), the hierarchy of growth time intervals is reversed from that shown in Figure 7. In other words, Δt is longer for $L_{\rm min}$ than for $L_{\rm max}$. This is again the result of the decrease in outflow velocity with increasing $T_{\rm eff}$, which occurs more strongly for larger stellar masses. Even in these cases, however, the variations in Δt between $L_{\rm nom}$ and $L_{\rm min}$ are well within the ranges noted above.

7. SIZES OF CIRCUMSTELLAR GRAPHITE AND TITANIUM CARBIDE GRAINS FORMED IN AGB STELLAR OUTFLOWS

In this section we use a simple kinetic model to predict maximum diameters for graphite and TiC as a function of stellar mass and effective temperature, taking into account the drift of dust with respect to gas in the stellar outflow. We also calculate gas pressures $P(T)$ in order to compare these results with the thermodynamic condensation sequence discussed in § 5. At the outset, is important to note that we are explicitly interested here in evaluating whether graphite and TiC grains of the sizes observed for presolar grains of these species can be produced by CV stars with the temperatures and luminosities depicted in the H-R diagram (Fig. 1), i.e., before they have reached the very end of their evolution and have departed from the AGB. Rather than attempting to present a "realistic" chemical kinetics model, we deliberately bias our kinetics calculations in favor of producing the largest grains that the mass outflows could possibly permit. We take this approach because of the considerable uncertainties associated with sticking efficiencies and other microscopic growth parameters, and also because the KFC1 presolar graphites are atypically large compared with the ~100 nm grain size thought to characterize grains in the ISM.

We begin by noting that the growth rate dr/dt of a grain is proportional to the speed v and the number density n_i of the gas species i contributing to its growth (see Clayton & Wickramasinghe 1976; Sharp & Wasserburg 1995):

$$\frac{dr}{dt} = \frac{\mu_s}{4\rho N_{\rm A}} n_i v, \tag{9}$$

where r, ρ, and μ_s are the grain radius, density ($\rho_{\rm graphite} = 2.25$ g cm^{-3}, $\rho_{\rm TiC} = 4.91$ g cm^{-3}), and molecular weight of the condensate, respectively, and $N_{\rm A}$ is Avogadro's number. Equation (9) assumes that the gas molecules contributing to grain growth stick with unit efficiency and do not subsequently evaporate. This means that the grain growth is limited only by the rate at which these molecules impact the surface, so the growth rate is *strictly maximal* under the given conditions of temperature, pressure, and number density of contributing molecules. Equation (9) is valid for monatomic solids (graphite in this case), as well as for the growth of diatomic solids in which the abundance of one atomic species in the gas phase is far smaller than the other and thus limits the rate of grain growth (Bernatowicz et al. 1996). This is the case for the TiC grains whose growth is modeled here: for a mean C/O of 1.15 (§ 5), the ratio of Ti to available C (i.e., carbon not tied up in CO molecules) is Ti/(C − O) ~ 6.7×10^{-4} in a gas having solar composition except for C (Anders & Grevesse 1989). Since the abundances of C and O are nearly equal for the cases we consider here, and since it is the *difference* in their abundance that appears in the denominator, the ratio Ti/(C − O) is highly sensitive to even small changes in the relative abundances of C and O.

The collision frequency of gas molecules with the grain, and the number of molecules needed to complete a new surface layer, are both proportional to the grain area, so the growth rate dr/dt in equation (9) is independent of the size of the grain. We ignore the difficult question of nucleation. For simplicity, we assume that equation (9) is valid once nuclei are present, and also assume that these nuclei are small compared to the size of the completely developed grain. We also ignore depletion of the gas species contributing to the growth, so as to maximize the grain size. In the present context, the speed v at which gas species of mass m_i arrive at grain surfaces is determined in part by their average kinetic molecular speed $\bar{v}_i$ for gas temperature T, where

$$\bar{v}_i = \left(\frac{8kT}{\pi m_i}\right)^{1/2}, \tag{10}$$

as well as by the drift speed $v_{\rm drift}$ of grains relative to the gas in the stellar mass outflow. For the temperature range we are considering ($T \sim T_G = 1800$–1000 K), $\bar{v}_i \sim 1$ km s^{-1} for the gas species (C_2H_2 for graphite, Ti [gas] for TiC) contributing to the growth. Following Habing et al. (1994), we find the drift speed from

$$v_{\rm drift} = \left[\frac{QLv(R)}{c\dot{M}}\right]^{1/2}, \tag{11}$$

where Q is the flux averaged momentum transfer efficiency, here taken as $Q \sim 0.03$ for carbon AGB stars (Schöier & Olofsson 2001), L is the luminosity, $v(R)$ is the gas outflow

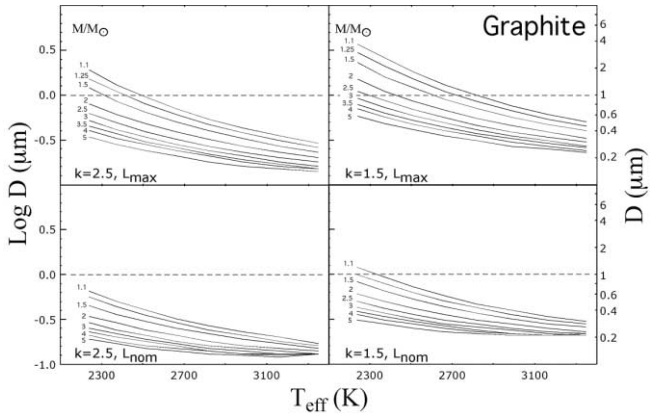

FIG. 8.—Maximum diameters of circumstellar graphite grains (in μm) as a function of effective temperature and stellar mass, for spherically symmetric AGB mass loss. Diameters for nominal stellar luminosity $L_{\rm nom}$ are shown in the bottom panels, and for maximum luminosity $L_{\rm max} = 2.35L_{\rm nom}$ in the top panels. The effect of the velocity field power index k is displayed for $k = 2.5$ (optically thick outflow; *left panels*) and $k = 1.5$ (optically thin outflow; *right panels*). For $L_{\rm max}$, the effective temperature T is taken to be the nominal effective temperature minus 200 K ($T = T_{\rm eff} - 200$ K). See text for discussion.

speed at radius R, $\dot{M}$ is the mass-loss rate, and c is the speed of light. For a given luminosity, $v_{\rm drift}$ increases with effective temperature because of the decrease in $\dot{M}$ with increasing $T_{\rm eff}$ (eq. [4]). We estimate the relative speed v with which gas molecules impinge on the surface of growing grains using

$$v = [(\bar{v}_i)^2 + (v_{\rm drift})^2]^{1/2}. \qquad (12)$$

The number density of gas species i at radius R is $n_i(R) = f_i n(R)$, where $n(R)$ is the gas number density at R and f_i is the number fraction of species i. For a C/O ratio representing the mean astronomical value for CV stars of C/O = 1.15 (§ 5), the number fraction of available carbon is $f_{\rm C} = 2.14\times10^{-4}$ and the number fraction of Ti is $f_{\rm Ti} = 1.44\times10^{-7}$, which implies an abundance ratio $f_{\rm C}/f_{\rm Ti} = 1.49\times10^{3}$.

If we write equations (3a)–(3c) in terms of $n(R)$ as $\dot{M} = 4\pi R^2(\mu/N_{\rm A})n(R)v(R)$ and express the infinitesimal time interval dt in the form $dt = dR/v(R)$, we may use equation (9) to find the grain size as a function of R:

$$r = r_0 + \frac{\mu_s}{\mu}\dot{M}\frac{f_i}{16\pi\rho}\int_{R_{1800\ \rm K}}^{R_{1000\ \rm K}} \frac{v}{R^2[v(R)]^2}\,dR, \qquad (13)$$

where v and $v(R)$ are given by equations (12) and (7), respectively, and $R(T)$ is given by equation (6). As noted above, we assume that $r_0 \ll r$, so it is set to zero in our solutions of equation (13).

The results of our growth calculations for graphite, obtained by numerical integration of equation (13), are displayed in Figure 8. We characterize the grain sizes in terms of their diameters $D = 2r$, rather than their radii, because the diameters of presolar graphite grains are more often quoted in the literature. As noted above (§ 6), we expect all graphite grains formed at maximum luminosity to survive, as well as at least some of the grains formed at nominal luminosity. We therefore show results for these two cases in Figure 8 as a function of the velocity field power indices for optically thin ($k = 1.5$) and optically thick ($k = 2.5$) outflows. The mean diameter of KFC1 presolar graphite spherules is in the range $\sim$1–2 μm (Paper I), and we indicate the grain size benchmark of 1 μm as a dashed line in Figure 8.

It is clear that even under the most favorable assumptions (perfect sticking efficiency, no evaporation, no depletion of gas species contributing to grain growth), graphite growth to $\sim$1 μm diameter is effectively impossible for nominal stellar luminosities and smooth, spherically symmetric outflows for even the smallest stellar masses that are relevant here (Fig. 8, *bottom two panels*). The situation is somewhat more favorable for maximum luminosities and optically thin outflows (*top right panel*), but even here the production of micron-sized graphite under optimal conditions is restricted to small stellar masses ($\lesssim$2.5 $M_\odot$). On the other hand, Amari et al. (2004) note that the light carbon isotopic composition of most KFC1 graphites, plus large excesses in ^{46}Ti and ^{49}Ti relative to ^{48}Ti in many grains (§ 2), is consistent with their origin around carbon stars of $M \gtrsim 3\ M_\odot$. From these results it is evident that under *realistic* growth conditions, micron-size graphite grains are not produced in AGB outflows that are smooth and spherically symmetric. However, smooth and spherically symmetric outflows may well produce much smaller, submicron-sized graphite grains.

Since the grain diameter in equation (13) is proportional to the number fraction f_i of the gas-phase species contributing to the growth, analogous results for TiC are readily estimated (assuming, rather unrealistically, that TiC will continue growing all the while that graphite does) by multiplying the results shown in Figure 8 by the ratio of the number fraction $f_{\rm Ti}$ of Ti to number fraction $f_{\rm C}$ of available carbon. For example, the maximum graphite diameter shown in Figure 8 is $D_{\rm graphite} = 3.7$ μm; therefore the maximum TiC diameter is given by $D_{\rm graphite}(f_{\rm Ti}/f_{\rm C}) \sim 2.5\times10^{-3}$ μm or $\sim$2.5 nm (a formal calculation using eq. [13] gives 2.8 nm). However, we note here that this calculation is inadequate for estimating the diameter of TiC. The velocity field (eq. [7]) that is used in equation (13) implicitly assumes that the condensing grains can couple effectively to the gas and thus drive the mass outflow from the star. This is expected to be the case when graphite grains form, but is unlikely to be the case for TiC, where the low abundance of Ti ($f_{\rm Ti}/f_{\rm C} = 6.7\times10^{-4}$) limits the number of TiC grains. We emphasize that the presolar TiC grains under discussion are those found inside of graphite, either having served as heterogeneous nuclei for graphite condensation or having been captured by and subsequently sequestered in growing graphite (Paper I). This means that in an earlier part of their growth history, these preexisting TiC grains would have been part of a somewhat lower velocity gas outflow at smaller radii and higher temperatures. Only for the later part of their growth history would they have shared the growth environment of graphite and thus the dynamical conditions under which graphite grows, namely, the greater accelerations and higher velocities in the graphite/gas outflow. Thus, the formation intervals displayed in Figure 6 will underestimate the time available for TiC growth. However, we can estimate the magnitude of the additional growth time interval from the following considerations.

Constraints on the relative condensation temperatures of TiC and graphite imposed by equilibrium thermodynamics for gas with C/O $\sim$ 1.1 imply that if TiC condenses prior to graphite (as it must in order to conform to the laboratory observations; Paper I), the maximum difference between the temperature of TiC condensation ($\lesssim$1800 K) and initial graphite condensation ($\sim$1670 K) is $\sim$130 K (see § 5, Fig. 2). For mass continuity in a spherically symmetric outflow, equations (3c) and (6) require that $v(1800\ {\rm K})/v(1670\ {\rm K}) \sim 1.5\,P(1670\ {\rm K})/P(1800\ {\rm K})$. Using results from Jørgensen et al. (1992) for spherical carbon star model atmospheres without grains, we find typical pressure

gradients in this temperature range of $P(1670\ \mathrm{K})/P(1800\ \mathrm{K}) \sim 0.4$, which thus give $v(1800\ \mathrm{K})/v(1670\ \mathrm{K}) \sim 0.6$. If the outflow speed $v(1670\ \mathrm{K})$ at the condensation temperature of graphite is assumed to be $v \sim 0.1 v_e$ (see discussion of eq. [7], § 6), we can determine the average velocity of grains in the temperature interval 1800–1670 K, as well as the additional average time that the grains take to travel to the radius where graphite will condense. Under the same conditions that give rise to the largest graphite grains (smallest effective temperature and maximum luminosity; see Fig. 8, *top right panel*), and taking into account the drift of grains with respect to the gas (eq. [11]), we find that the growth times shown in Figure 6 are extended by ~2, ~3, and ~4 yr for stars of 1.1, 2.5, and 5 $M_\odot$, respectively. This gives total TiC diameters of ~18, ~4, and ~1.4 nm, with the time intervals between initial TiC and graphite condensation accounting for 84%, 72%, and 50% of the final TiC diameters in these three cases. The calculated TiC diameters may be compared with the observed mean TiC diameter in KFC1 graphites (24 ± 14 nm; Paper I). It is clear that only TiC grains formed around carbon stars of the smallest possible mass (~1.1 $M_\odot$) fall within the observed range. And, for the stars that are the likely source of presolar graphite (with $M \gtrsim 3\ M_\odot$), the calculated diameters for spherically symmetric outflows fall an order of magnitude or more short of accounting for the observations even under the most favorable growth conditions. This conclusion can be extended readily to the other types of carbides, for example solid solutions of ZrC with TiC, that have been observed as internal crystals in KFC1 graphites (Bernatowicz et al. 1996; Paper I). The solar abundance of Zr is ~200 times less than the abundance of Ti, and presumably the only reason that we find internal crystals of such carbides within circumstellar graphite is because of the *s*-process enrichment of Zr (Paper I) that occurs in the He-burning shells of AGB stars. Even with such enrichment, however, it is clear that formation and growth of such carbides in smooth and spherically symmetric circumstellar outflows is just as difficult as the formation of pure TiC.

In the kinetics calculations above, we have used solar abundances from the Anders & Grevesse (1989) compilation, but recent compilations have predicted a lower fractional abundance of C and O. Of relevance to the present work are the abundances of C, O, and Ti. In the recent compilation of Lodders (2003), for example, the fraction of available carbon of f_C is lowered by a factor of ~1.7, which therefore reduces the maximum diameters in the above calculations from 3.7 to 2.2 μm for graphite. However, the solar C/O and f_{Ti} are essentially unchanged, meaning that the maximum calculated TiC diameters, as well as the results of the thermodynamic condensation calculations shown in Figure 2, are unaffected.

We may now compare total gas pressures implied by the above calculations to pressures required to form TiC prior to graphite by equilibrium thermodynamics, because for a given growth interval Δt, the grain diameter is proportional to the pressure. Taking the most favorable conditions for growth of TiC discussed above, we calculate $P \sim 0.03$, ~0.005, and ~0.001 dynes cm^{-2} when graphite begin to condense, for stars of 1.1, 2.5, and 5 $M_\odot$, respectively. These pressures are factors of ~100 to ~3000 times smaller than the minimum equilibrium pressure (~3 dynes cm^{-2} at C/O ~1.1) needed for formation of TiC prior to graphite. The pressure shortfalls are 1–2 orders of magnitude larger than shortfalls in grain size, and they vary for different solar masses because of the differences in the extended atmosphere structure. The pressure shortfalls are larger than the grain-size shortfalls, in part due to the to the perfect growth conditions assumed in the grain growth calculations. Nonetheless, the predictions of growth kinetics and of equilibrium thermodynamics are qualitatively consistent with one another.

If it were not for the fact that demonstrably circumstellar grains of micron-sized graphite are available for study in the laboratory, we would likely have inferred that only submicron-sized graphite grains can be produced in AGB circumstellar outflows, and would certainly not have predicted the occurrence of refractory Ti carbides inside of them. Yet, such grains *do* exist, and we are therefore required to account for them. However, note that the inability to account for graphite and TiC of the requisite sizes and the inability to account for the formation of TiC prior to graphite result ultimately from the assumption that AGB outflows are smooth and spherically symmetric. The mass-loss rate for symmetrically distributed circumstellar matter is simply too small to produce gas pressures large enough to enable growth of grains of the sizes required and to form grain species in the correct sequence (§ 5). Clearly, we are forced to abandon the assumption of the uniform, spherically symmetric outflow in order to make further progress.

A hint that this is the necessary resolution to the pressure/grain size problem comes from the astronomical observation of the carbon stars with the highest mass-loss rates (with $\dot{M} > 2.5 \times 10^{-5}\ M_\odot\ \mathrm{yr}^{-1}$) that appear to constitute a distinct group in Figure 4. If the mass outflows from this group of late-stage AGB stars resemble that of their well-studied member IRC +10216 (§ 6), then they are plausibly temporally variable, nonhomogeneous, and nonsymmetrical, with clumps and/or jets of high density. As pointed out by Bernatowicz et al. (1996), there is other substantial astronomical evidence, e.g., from maser emission, of density clumps in circumstellar envelopes. We will not speculate here on the physical causes of outflow inhomogeneity, but its relevance to the grain growth problem that we have been considering is clear. The advantage that this physical configuration poses is relaxation of the specific coupling between overall stellar mass-loss rate and local gas density that is implicit in spherically symmetric configurations. In particular, regions of enhanced density in the outflow with small angular scales could permit growth of large grains without at the same time requiring mass-loss rates far larger than are observed. To illustrate this point, we note that the maximum observed mass-loss rate for CV stars is $\sim 10^{-4}\ M_\odot\ \mathrm{yr}^{-1}$ (Fig. 4), which is $\dot{M}/4\pi \sim 10^{-5}\ M_\odot\ \mathrm{yr}^{-1}\ \mathrm{sr}^{-1}$. Let us suppose that, from a star with this integrated mass-loss rate, matter is ejected at a rate $\dot{m}$ through each of 10 randomly oriented areas subtending equal solid angles Ω. Then $(\dot{m}/\Omega)(\Omega/4\pi) \sim 10^{-6}\ M_\odot\ \mathrm{yr}^{-1}\ \mathrm{sr}^{-1}$. If each area is assumed to subtend a fractional solid angle $\Omega/4\pi \sim 10^{-4}$ [i.e., $\Omega \sim (2^\circ)^2$], this corresponds to $\dot{m}/\Omega \sim 10^{-2}\ M_\odot\ \mathrm{yr}^{-1}\ \mathrm{sr}^{-1}$. Thus, with regard to conditions responsible for the growth of grains in these areas, it is as if the mass-loss rate for a spherically symmetric distribution had been effectively magnified by a factor of 1000.

Stars near the end of their evolution on the AGB with mass-loss rates $\sim 10^{-4}\ M_\odot\ \mathrm{yr}^{-1}$ are perhaps the most plausible candidates for the growth of micron-sized graphite grains and/or graphites with internal carbide crystals. However, since the same considerations apply, it is also possible that local density enhancements (clumpiness) in the mass outflows of stars during their normal residence on the AGB could produce such grains as well.

8. SUMMARY AND CONCLUSIONS

We have used laboratory data on presolar graphite grains in conjunction with astronomical observations to infer grain formation conditions in the mass outflows from carbon AGB stars.

The laboratory data on the isotopic compositions of noble gases, Ti, and C in KFC1 graphites point to an origin in AGB stars. Thermochemical calculations indicate that the parent stars must have C/O > 1, because the available oxygen will be tied up in CO molecules, leaving only the remaining C available for the formation of carbonaceous grains. The source of the graphite grains must therefore be carbon AGB stars. We derived the minimum mass for stars that could contribute presolar grains to the solar nebula, and we used this result, along with a mass-luminosity relation inferred from observations of carbon stars, to identify the region of the H-R diagram relevant to the production of presolar graphite.

The occurrence of TiC crystals within a subset of the graphite grains indicates the formation of TiC prior to graphite. Because equilibrium thermodynamics correctly predicts the C/O ratios observed astronomically in variable carbon (CV) stars, we can use it to infer the pressures and temperatures necessary to form TiC prior to graphite formation in circumstellar outflows. The inferred pressures, coupled with observed outflow velocities from carbon stars, lead to inferred mass-loss rates for spherically symmetric outflows that are much too large in comparison with those derived from astronomical observation.

We used the results of equilibrium thermodynamics and kinetics calculations to infer a maximum plausible temperature range over which TiC and graphite grains could form (1800–1000 K). This temperature range, in conjunction with mass-loss rate formulae and velocity fields derived from detailed dynamical models, leads to estimates for condensation radii of 2.3–3.7 AU and grain growth times on the order of several years, for stars in the 1.1–5 $M_{\odot}$ range with effective temperatures from 2240 to 3350 K. These results are independent of any considerations of grain size.

Using strictly optimal conditions for grain growth, we performed growth kinetics calculations to investigate whether graphite grains and TiC grains of the mean sizes observed for these presolar species (1–2 μm and 24 nm, respectively) could be grown in spherically symmetric AGB outflows. We found this highly unlikely for both graphite and TiC. The observed mass-loss rates for carbon stars are simply too small to permit the growth of presolar graphite and TiC grains of the sizes observed, if the mass loss is constrained to be spherically symmetric. This is simply the complement of the conclusion based on the pressure requirements imposed by equilibrium thermodynamics.

However, we *do* have examples of such circumstellar grains in hand, so it must nonetheless be possible for nature to produce them. We therefore take the above results to indicate that the assumption of smooth and spherically symmetric outflows from carbon AGB stars is not valid, at least with regard to the stellar sources of presolar graphite grains. Instead we must conclude, on the basis of pressures inferred from equilibrium thermodynamics, as well as from calculations of the kinetics of grain growth, that the matter from the carbon star sources of presolar graphite is ejected in spatially discrete clumps or jets that have small angular scales. This conclusion derives support, among other astronomical data, from observations of the nearby carbon star IRC +10216.

As discussed in Paper I, the enrichment of ^{12}C in many KFC1 graphites, and the overabundances of the *s*-process elements Mo, Zr, and Ru in the carbides found within them, often greatly exceed the values observed astronomically in AGB outflows. These observations not only lend further support to the idea that the outflows are clumpy, but also imply that the outflowing matter is not well mixed in the circumstellar envelope out to the radii where grain condensation takes place. Furthermore, the scale of the compositional inhomogeneities appears to be significantly smaller than the spatial resolution of current astronomical observations of AGB outflows.

This work arose initially out of discussions with Larry Grossman (University of Chicago) and benefited from helpful suggestions by Xander Tielens (Kapteyn Astronomical Institute) and an anonymous reviewer. This work was partially supported by NASA under contract NNG04GG13G, issued through the Office of Space Science.

REFERENCES

Amari, S., Lewis, R., & Anders, E. 1994, Geochim. Cosmochim. Acta, 58, 459
———. 1995, Geochim. Cosmochim. Acta, 59, 1411
Amari, S., Nittler, L. R., Zinner, E., Gallino, R., Lugaro, M., & Lewis, R. 2001, ApJ, 546, 248
Amari, S., Zinner, E., & Lewis, R. S. 2004, Meteoritics Planet. Sci., 39, 5152
Anders, E., & Grevesse, N. 1989, Geochim. Cosmochim. Acta, 53, 197
Arndt, T. U., Fleischer, A. J., & Sedlmayr, E. 1997, A&A, 327, 614
Bennett, C. L., et al. 2003, ApJS, 148, 1
Bergeat, J., Knapik, A., & Rutily, B. 2001, A&A, 369, 178
———. 2002a, A&A, 390, 967
———. 2002b, A&A, 390, 987
Bergeat, J., & Sibai, A. M. 1983, A&A, 119, 207
Bernatowicz, T. J., & Cowsik, R. 1997, in AIP Conf. Proc. 402, Astrophysical Implications of the Laboratory Study of Presolar Materials, ed. T. J. Bernatowicz & E. Zinner (New York: AIP), 451
Bernatowicz, T. J., Cowsik, R., Gibbons, P., Lodders, K., Fegley, B., Amari, S., & Lewis, R. 1996, ApJ, 472, 760
Bernatowicz, T. J., Messenger, S., Pravdivtseva, O., Swan, P., & Walker, R. M. 2003, Geochim. Cosmochim. Acta, 67, 4679
Bernatowicz, T. J., & Walker, R. M. 1997, Phys. Today, 50(12), 26
Bernatowicz, T. J., & Zinner, E., eds. 1997, AIP Conf. Proc. 402, Astrophysical Implications of the Laboratory Study of Presolar Materials (New York: AIP)
Bessell, M. S., Scholz, M., & Wood, P. R. 1996, A&A, 307, 481
Bowen, G. H. 1988, ApJ, 329, 299
Chigai, T., Yamamoto, T., & Kozasa, T. 2002, Meteoritics Planet. Sci., 37, 1937
Clayton, D. D., & Nittler, L. R. 2004, ARA&A, 42, 39
Clayton, D. D., & Wickramasinghe, N. C. 1976, Ap&SS, 42, 463
Croat, T. K., Bernatowicz, T. J., Amari, S., Messenger, S., & Stadermann, F. 2003, Geochim. Cosmochim. Acta, 67, 4705
Croat, T. K., Stadermann, F., & Bernatowicz, T. J. 2005, ApJ, 631, 976 (Paper I)
Daulton, T. L., Bernatowicz, T. J., Lewis, R. S., Messenger, S., Stadermann, F. J., & Amari, S. 2002, Science, 296, 1852
———. 2003, Geochim. Cosmochim. Acta, 67, 4743
Feast, M. W., Robertson, B. S. C., Catchpole, R. M., Lloyd Evans, T., Glass, I. S., & Carter, B. S. 1982, MNRAS, 201, 439
Gallino, R., Busso, M., & Lugaro, M. 1997, in AIP Conf. Proc. 402, Astrophysical Implications of the Laboratory Study of Presolar Materials, ed. T. J. Bernatowicz & E. Zinner (New York: AIP), 115
Habing, H. J., Tignon, J., & Tielens, A. G. G. M. 1994, A&A, 286, 523
Hofmann, K.-H., Scholz, M., & Wood, P. R. 1998, A&A, 339, 846
Hoppe, P., & Ott, U. 1997, in AIP Conf. Proc. 402, Astrophysical Implications of the Laboratory Study of Presolar Materials, ed. T. J. Bernatowicz & E. Zinner (New York: AIP), 27
Iben, I. 1967, ApJ, 147, 624
Ivezic, Z., Knapp, G. R., & Elitzur, M. 1998, in Proc. Sixth Annual Conference of the CFD Society of Canada (Ottawa: CFDSC), IV-13
Jones, A. P., Tielens, A. G. G. M., Hollenbach, D. J., & McKee, C. F. 1997, in AIP Conf. Proc. 402, Astrophysical Implications of the Laboratory Study of Presolar Materials, ed. T. J. Bernatowicz & E. Zinner (New York: AIP), 595
Jørgensen, U. G., Johnson, H. R., & Nordlund, Å. 1992, A&A, 261, 263
Jura, M. 1994, ApJ, 434, 713
Krauss, L. M., & Chaboyer, B. 2003, Science, 299, 65
Lambert, D., Gustaffson, B., Eriksson, K., & Hinkle, K. 1986, ApJS, 62, 373
Lampens, P., Kovalevsky, J., Froeschlé, M., & Ruymaekers, G. 1997, in *Hipparcos*, Venice '97, ed. B. Battrick (ESA SP-402; Noordwijk: ESA), 421
Lodders, K. 2003, ApJ, 591, 1220
Lodders, K., & Fegley, B. 1995, Meteoritics, 30, 661

Lodders, K., & Fegley, B. 1997a, in AIP Conf. Proc. 402, Astrophysical Implications of the Laboratory Study of Presolar Materials, ed. T. J. Bernatowicz & E. Zinner (New York: AIP), 391
———. 1997b, ApJ, 484, L71
Martin, C., Mignard, F., Hartkopf, W. I., & McAlister, H. A. 1998, A&AS, 133, 149
Messenger, S., Keller, L. P., Stadermann, F. J., Walker, R. M., & Zinner, E. 2003, Science, 300, 105
Netzer, N., & Elitzur, M. 1993, ApJ, 410, 701
Nguyen, A. N., & Zinner, E. 2004, Science, 303, 1496
Nittler, L. R. 2003, Earth Planet. Sci. Lett., 209, 259
Perryman, M. A. C. 1997, The *Hipparcos* and Tycho Catalogues (ESA SP-1200; Noordwijk: ESA)
Sackmann, I. J., Boothroyd, A. I., & Kramer, K. E. 1993, ApJ, 418, 457
Schöier, F. L., & Olofsson, H. 2001, A&A, 368, 969
Sharp, C., & Wasserburg, G. J. 1995, Geochim. Cosmochim. Acta, 59, 1633
Soker, N., & Harpaz, A. 1999, MNRAS, 310, 1158
Stadermann, F. J., Croat, T. K., Bernatowicz, T. J., Amari, S., Messenger, S., Walker, R. M., & Zinner, E. 2005, Geochim. Cosmochim. Acta, 69, 177
Weigelt, G., Balega, Y., Blöcker, T., Fleischer, A. J., Osterbart, R., & Winters, J. M. 1998, A&A, 333, L51
Winters, J. M., Le Bertre, T., Jeong, K. S., Helling, Ch., & Sedlmayr, E. 2000, A&A, 361, 641
Zinner, E. 1998, Annu. Rev. Earth Planet. Sci., 26, 147